How Can Protons Migrate in Extremely Compressed Liquid Water?

Sho Imoto* and Dominik Marx
Lehrstuhl für Theoretische Chemie, Ruhr–Universität Bochum, 44780 Bochum, Germany

(Received 25 February 2020; accepted 24 July 2020; published 21 August 2020)

Compression of liquid water up to multi-kbar pressures is known to perturb dramatically its local structure required for charge defects to migrate as topological defects in the hydrogen-bonded network. Our *ab initio* simulations show that the migration of excess protons is not much affected at 10 kbar, whereas that of proton holes is significantly reduced. Non-Markovian analyses show that this is not due to modifying the free energy barriers of both charge transfer and migration. It is rather pressure-induced modifications of the population of activated states, depending on interstitial water, which rules charge migration at extreme compression.

DOI: 10.1103/PhysRevLett.125.086001

The migration, transport, and conductance of excess protons (H^+) and proton holes (OH^-) in aqueous environments are of widespread importance in science and technology. These processes are at the heart of energy conversion [1–3], aqueous solutions [4,5], and signal transduction [6,7] to name but a few examples. In particular, it has been rigorously established that their peculiar macroscopic transport kinetics are intimately connected to the microscopic structural dynamics of the specific topological defects created by excess protons or proton holes in the three-dimensional H-bond network structure of water [8,9].

As opposed to this extensive knowledge in case of essentially perfect H-bond water networks [4,5], our understanding of the transport properties of excess protons and proton holes in strongly perturbed such networks remains rather scarce [4,5]. Notable exceptions are quasi-1D carbon nanotubes and biological channels where the peculiarities of single-file proton conduction along H-bonded water wires have been studied in molecular detail [10–14]. Similarly, proton transfer across single-layer graphene at room temperature is observed through nanopinholes [15,16]. Furthermore, recent work on extremely narrow slit pores provided surprises as to the impact of 2D nanoconfinement on proton (hole) migration [17–20]. For instance, despite extreme perturbations of the H-bond network within ultranarrow monolayer slit pores, proton diffusion has been predicted [17] to still occur therein, as subsequently confirmed experimentally [21].

In stark contrast to such confinement-induced perturbations, however, it remains unknown if protons and their holes can still migrate in liquid water that has been compressed up to its stability limit, which is roughly 10 kbar at room temperature corresponding to a density as high as about 1.24 g/cm^3. At such extremely high hydrostatic pressures, it is well documented that the structure of liquid water is significantly changed compared to ambient [22,23]. Microscopically, the large void spaces within the open tetrahedral H-bond network get filled at 10 kbar by about two additional water molecules per reference molecule, thus allowing for the significant density increase. These so-called "interstitial water molecules" stay within the first hydration sphere but are not H bonded with the reference water [24,25]. Thus, they can be expected to reduce Grotthuss-like proton (hole) transfer [4,5] that occurs exclusively along H bonds and, therefore, impede charge transport. Moreover, interstitials are generating additional excluded volume within the respective hydration spheres, thus suggesting to furthermore hinder structural diffusion.

In an effort to elucidate the impact of such pressure-induced perturbations, we carry out extensive *ab initio* simulations [26] of H^+ and OH^- migration in water at 300 K, which has been compressed as much as possible while keeping it in the liquid state, namely, to 10 kbar. We find, in a nutshell, that migration of proton holes gets strongly suppressed at 10 kbar while the excess proton remains largely unaffected. This is not because of pressure-induced changes of free energy barriers, but due to suppressing activated states only in the case of OH^- while interstitials shield the activated protonic defect.

Structural H-bonding analysis.—Let us start by analyzing the local structure around the excess proton and proton hole in extremely compressed water in terms of their spatial distribution functions (SDFs) as provided by the well-established dispersion-corrected RPBE-D3 density functional (see Supplemental Material [27], Sec. I for computational details and Sec. II for a discussion of its validity specifically for the present application as well as for a concise digression on nuclear quantum effects). At normal pressure, the solvation structure of the H_3O^+ core of the localized topological (so-called Eigen) defect [4,5] features only the well-known three H bonds donated by its three H atoms, whereas its O atom (denoted as O^* in the following; see Fig. S1 for complete atom labeling [27]) is not involved at all in H bonding as depicted in Fig. 1(a). This solvation structure is nicely unveiled when using the so-called

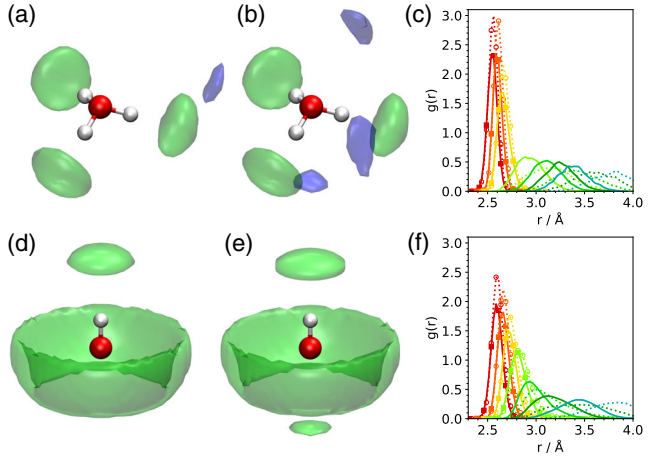

FIG. 1. Spatial distribution functions of H-bonded (green) and interstitial (blue) water molecules around H_3O^+ at (a) 1 bar and (b) 10 kbar in bulk water at 300 K. (c) Incremental radial distribution functions from 1st up to 7th neighbors (from red to yellow to green to blue) of H_3O^+ at 1 bar (dotted lines with additional open symbols to highlight the full first solvation shell) and 10 kbar (solid lines will filled symbols accordingly). Same spatial distribution functions around OH^- at (d) 1 bar and (e) 10 kbar and corresponding incremental radial distribution functions for OH^- (f). The SDF isovalues used correspond to the respective bulk densities of the solutions; note that interstitial water density is only seen in panel (b). The incremental RDFs are displayed in Fig. S2 [27] with more distant neighbors and in full size.

incremental radial distribution functions (RDFs) [52,53], where the total O^*—O RDF is decomposed into distributions due to the 1st, 2nd …, *n*th neighboring molecules (see Supplemental Material, Sec. III. B for more details [27]). As shown in Fig. 1(c) and Fig. S2(a) of Ref. [27], the distributions of the 1st to 3rd neighbors are very narrow, indicating a well-structured first solvation shell, whereas those beyond are characterized by rather broad distributions. What happens to that H-bond topology upon extreme compression? Our AIMD simulations at 10 kbar show that the average number of donated and accepted H bonds are still 3.0 and 0.1, respectively, which is identical to what is observed at 1 bar. However, novel features appear in the corresponding SDF as visualized by the blue isosurfaces in Fig. 1(b). Similarly to what is known for pure water [25] at 10 kbar, non-H-bonding water molecules, so-called interstitials, are squeezed into the void space that is offered at normal pressure in the first solvation sphere seen as the pronounced pressure-induced shift of the distribution of 4th neighbors in Fig. 1(c). Yet, the threefold H-bonding pattern known from 1 bar is perfectly conserved at 10 kbar [cf. green regions in panels (a) and (b) and the peaks due to 1st to 3rd neighbors in panel(c) which remain unaffected]. Supporting analyses of topology-resolved O^*—O RDFs in Fig. S3 demonstrate that these interstitials contribute a novel peak at 3.4 Å at 10 kbar unknown at 1 bar, which is caused by third and fourth topological neighbors in terms of the H-bond network connectivity [27]. In other words, the pressure perturbations change the H-bond network around the localized excess proton only at intermediate distances, whereas the local H-bonding pattern is virtually identical at 10 kbar compared to 1 bar.

What happens to OH^- upon extreme compression? At ambient conditions, the embedding of the localized proton hole, $(O^*H')^-$, in the H-bond network of water is established [4,54] by about four H bonds accepted by O^* and a minor contribution due to a donated H bond by H' as confirmed by our SDF in Fig. 1(d). Surprisingly, both the H-bond pattern and number change at 10 kbar, contrary to H^+ where only interstitials are created. There is now an enhanced propensity of OH^- to accept additional H bonds at O^* along the O-H axis (clearly seen in the SDF in Fig. 1(e) by the lower blob) while the equatorial ring, already densely populated at 1 bar, remains essentially unaffected. Moreover, the number of accepted (donated) H bonds increases from about 4.5 (0.7) at 1 kbar to roughly 4.8 (0.9) at 10 kbar, implying that OH^- is engaged in as many as six H bonds in total after extreme compression. Very unexpectedly, there are no interstitial water molecules found despite the large void space that is offered at 1 bar. In other words, the solvation shell around OH^- is compressed uniformly as evidenced by the rather insignificant overall pressure shifts of the incremental RDFs in Fig. 1(f) which only leads to the increased number of H bonds. Thus, that open space in between the O^* and H' sites is preserved at 10 kbar since no topological third and fourth neighbors are found to squeeze in (as supported by topological radial analysis in Fig. S3 [27]). This astonishing phenomenon will greatly impact on proton hole migration at 10 kbar as worked out below.

We conclude that the 10 kbar pressure response of topological defects in the H-bond network due to localized excess protons and proton holes is qualitatively very different, both concerning the H-bond pattern and interstitial water molecules.

Qualitative insights.—Given their distinctly different structural pressure responses, we are now going to focus on the proton (hole) migration at high pressure conditions with reference to normal pressure. For the purpose of illustration only, representative 50 ps pieces sampled from the full trajectories (of 1.1 and 1.4 ns duration after equilibration for H^+ and OH^-, respectively, on which all subsequent analyses are based) in order to trace the O^* index of the four systems as depicted in Fig. 2(a). Although no quantitative conclusions are intended at this stage, the number of proton transfer events of H^+ at 1 bar and 10 kbar is very similar (top two panels). In stark contrast, the behavior of OH^- turns out to be distinctly different at extreme pressure: There are much fewer proton hole transfers observed at 10 kbar compared to 1 bar (bottom two panels). Recalling the structural (SDF and RDF)

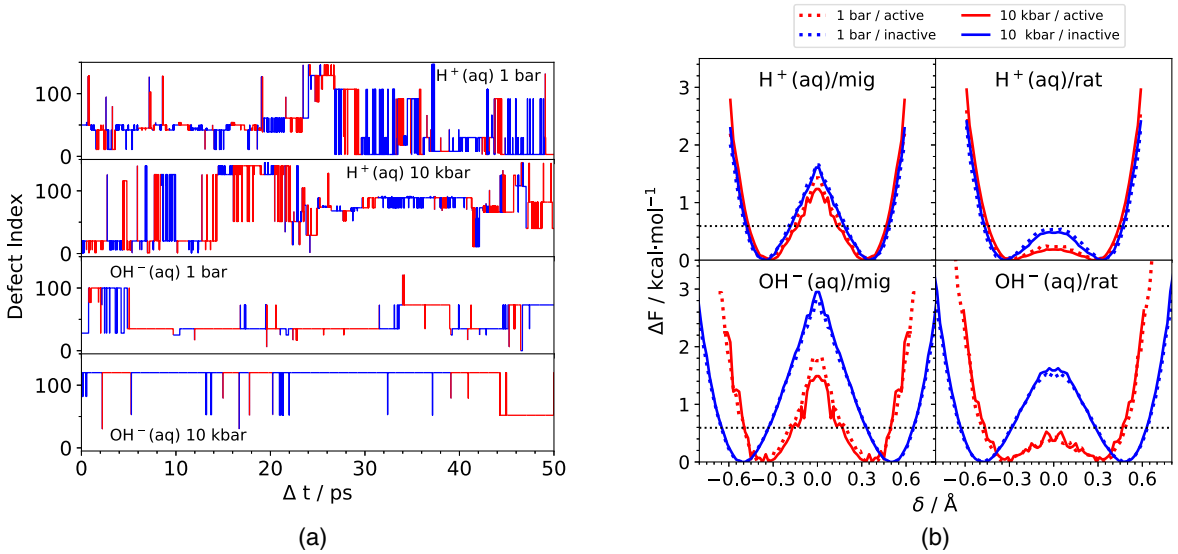

FIG. 2. (a) Representative continuous trajectory pieces for proton (hole) migration at 10 kbar versus 1 bar as monitored by the index of the O^* site, see text. All migration events according to our non-Markovian analysis (using a memory length of $N_{\max} = 3$, see text and SI Sec. IV [27]) are indicated by (blue $\leftrightarrow$ red) color changes, thus implying rattling periods in between if only the O^* site changes without concurrent color change. The number of successful proton (hole) migration events (thus excluding local rattling) in these trajectory fragments is 61, 59, 16, and 7 for H^+ at 1 bar, H^+ at 10 kbar, OH^- at 1 bar, and OH^- at 10 kbar, respectively. (b) Free energy profiles along the δ coordinate at 10 kbar (solid lines) and 1 bar (dashed lines) from non-Markovian analysis (using $N_{\max} = 3$) for proton (hole) defects dissected in terms of migration (left panels) and rattling (right panels) processes combined with the respective topological defects being in active (red lines) or inactive (blue lines) states. The horizontal dotted lines mark the thermal energy k_BT at 300 K.

analyses, this is not only surprising but also counterintuitive in view of much interstitial water being squeezed into void space around the excess proton, see blue regions in Fig. 1(b), thus creating excluded volume therein, whereas that void space remains unblocked close to the proton hole, see panel 1(e).

Free energy profiles.—How can this unexpected behavior be possibly explained? Concerning proton (hole) migration, it is firmly established that many proton (hole) transfer events do not lead to long-range transport but only to local rattling motion in a given H bond and thus do not contribute to diffusion [4,8,9]. To disentangle these two processes at the level of free energies, we perform a non-Markovian analysis as follows. A transfer event is considered as rattling when the new O^* site had already accepted the proton (hole) within the latest $N_{\max} - 1$ transfer events, while all other transfer events are categorized as migration (see SI Sec. IV of the Supplemental Material [27] for the protocol where it is also shown that convergence of this analysis is fast and that a memory length of $N_{\max} = 3$ captures the relevant trends). As illustrated by Fig. 2(a), all proton (hole) transfer events are nicely distinguished in terms of ratting and migration. Second, it is also well known that proton (hole) transfer along the so-called δ coordinate (see Supplemental Material [27]) preferentially occurs within specific local H-bond patterns around the topological defect [4,8,9]. In the case of H^+ in water, excess proton transfer is triggered when the proton-receiving water molecule (given by $\tilde{O}$ as defined in Fig. S1) loses one accepted H bond and, thus, becomes an undercoordinated water molecule (see Supplemental Material [27], Sec. III.A for background). On the other hand, proton hole transfer occurs readily when one of the typically four H bonds of the proton-receiving O^* site of OH^- gets broken (see Supplemental Material [27], Sec. III.A). Hereafter, we call these structures "active" versus the "inactive" resting state structures.

Based on these considerations, we are able to fully dissect the total free energy profiles along the charge transfer coordinate δ in terms of long-distance charge defect migration versus local rattling processes within active and inactive local H-bonding patterns at 10 kbar compared to 1 bar, see Fig. 2(b). First of all, it is reassuring to confirm for the excess proton at ambient pressure that the free energy barrier of proton rattling (top right panel), which does not contribute to charge transport and thus conductivity, is below the thermal energy of $\approx$0.6 kcal/mol at 300 K as expected [4,8,9]. Moreover, our present non-Markovian analysis also confirms that long-distance proton transport in liquid water at ambient conditions [4,8,9] (i) is a thermally activated process (ii) that requires the aforementioned specific H-bonding structure of the charge defect since (i) migration in active states features a barrier of $\approx$1.5 kcal/mol that clearly exceeds the thermal energy, and (ii) an even higher barrier for migration within inactive states [top left panel in Fig. 2(b)].

In case of proton holes in ambient water, ratting within active H-bonded structures is essentially barrierless (bottom right panel), whereas these active states allow for proton hole migration processes subject to an activation barrier of about 2 kcal/mol (bottom left) which is higher than that for the migration of excess protons. Moreover, the barrier for proton hole migration within inactive H-bonding states is found to be considerably higher (by ≈1 kcal/mol) than for the same process in active states, whereas that difference is merely 0.3 kcal/mol in the case of the excess proton. These energetics correlate with the structural analyses in Fig. S5 of Ref. [27]: The average $O^* \cdots \tilde{O}$ distance is essentially identical in active and inactive states in case of the excess proton, whereas a sizable shortening of that critical intermolecular distance (see Fig. S1 in the Supplemental Material [27]) is observed in active H-bonding states of the proton hole relative to its inactive states. In other words, the correct local H-bond structure around the charge defect is much more crucial for proton hole migration than for the migration of excess protons. We conclude that our non-Markovian analysis provides molecular scenarios that are in full agreement with the well-established mechanisms of both the excess proton and proton hole transport in ambient water [4,8,9].

Having demonstrated that non-Markovian analysis works for charge migration in liquid water at ambient conditions [4,8,9], we are confident to apply it now to extremely compressed liquid water. Expecting here stark pressure-induced differences in view of the previous structural and trajectory analysis, it is utmost puzzling to find out that all free energy profiles at 10 kbar are essentially identical to those at 1 bar according to Fig. 2(b). In other words: Pressure effects on the activation free energies for both local charge transfer and long-range charge migration cannot explain the stark differences observed. This finding is qualitatively in line with the underlying sub-ps fluctuations of the H-bond network of liquid water—and thus the relevant electric field fluctuations—being largely pressure insensitive even up to 10 kbar as revealed by THz spectroscopy [55,56].

Local H-bonding analysis.—To solve this paradox, we now unveil crucial effects due to changes in the local H-bonding patterns of the proton-receiving oxygen site (i.e., $\tilde{O}$ for H_3O^+ and O^* for OH^- as shown in the insets) by dissecting the population of active and inactive states in Fig. 3. Recall that H_3O^+/OH^- gets activated for proton (hole) transfer once $\tilde{O}/O^*$ transiently accepts only one (three H bonds) due to thermal fluctuations [4,8,9]. In the case of the excess proton, the H-bonding pattern of $\tilde{O}$ remains similar upon compression from 1 bar to 10 kbar and, importantly, the relative population of the active state remains high, about 50%. In stark contrast, the H-bonding pattern around the O^* site of the proton hole is much more sensitive to pressure perturbations. In particular, the population of active states decreases by a factor of 2, from 4.3% at 1 bar to 2.1% at 10 kbar. This can be rationalized in the

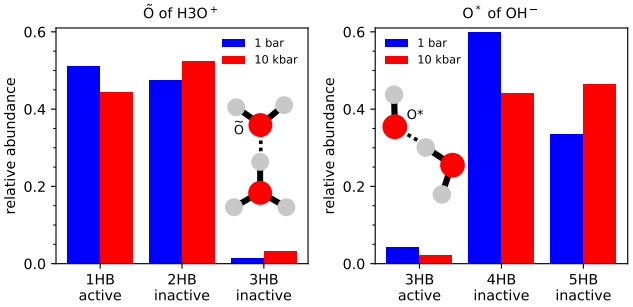

FIG. 3. Normalized number of accepted H bonds around the proton-receiving oxygen sites at 10 kbar and 1 bar, being the $\tilde{O}$ site of H_3O^+ (left) and the O^* site of OH^- (right), as defined by the insets (see also Fig. S1 [27]).

light of the previous SDF analysis: The fact that no interstitial water molecules are found around the proton hole defect even at 10 kbar, compare Fig. 1(e) to 1(d), implies that this void space remains available to accept *additional* H-bonding water molecules instead. This crowded H-bonded state at 10 kbar blocks OH^- for proton migration because that requires a *reduction* of accepted H bonds at O^* instead. This is not possible in case of H^+ where the void space gets largely blocked by non-H-bonded interstitials.

We conclude that only a tiny fraction of the OH^- defect states remains prepared for proton hole transfer at 10 kbar, whereas the overwhelming majority is inactive in view of OH^- accepting too many H bonds as a result of compressing the liquid. Based on this analysis, we attribute the slowing down of proton hole migration at extreme pressures to the significantly suppressed relative population of active states whereas the excess proton is not much affected due to an enhanced population of interstitial water. This result clearly indicates the salient impact of interstitials on the local H-bonding pattern around the proton (hole) charge defects and, thus, on the transport properties of acidic (alkaline) aqueous solutions in the limit of extreme hydrostatic compression.

Conclusions and outlook.—Our *ab initio* simulations unveil a distinctly different pressure response of the migration of excess protons versus proton holes in liquid water. While the former process remains essentially unaffected at 10 kbar compared to ambient, proton hole migration is found to be strongly suppressed. This phenomenon is not due to pressure modifying the involved free energy barriers, which remain close to invariant, but due to greatly suppressing the population of active states only in case of proton hole defects. Phenomenologically speaking, the qualitatively different pressure responses of positive and negative charge defects in liquid water will enhance the separation of cationic and anionic conductivity constituents, rendering the cationic one even more predominant at multi-kbar pressures. Measuring the overall conductivity of aqueous solutions as a function of pH at

extreme hydrostatic versus ambient pressure would be a way to quantify that pressure-induced change. Second, there are no interstitial (i.e., non-H-bonded) water molecules found in the void space around the proton hole, very differently from what is seen for the excess proton. Overall, leaving lots of unoccupied void space at 10 kbar and thus accessible volume leads to an enhanced propensity of OH^- to accept additional H bonds, which directly counteracts the required activation of the proton hole for migration. In stark contrast, the excluded volume generated due to interstitials even stabilizes the active states of H^+ by blocking the formation of additional H bonds. It might be worth as a refinement to quantify in future work the effects we discovered using quasiclassical (centroid or ring polymer) path integral *ab initio* simulations. In conclusion, the distinctly different pressure response of alkaline versus acidic aqueous solutions at very high pressures—where water still is a liquid—will broadly impact charge transport, mobility, and conductivity in extreme aqueous environments.

We thank Stefan Kast (TU Dortmund) and Janos Daru (Bochum) for helpful discussions. Funded by the Deutsche Forschungsgemeinschaft (DFG, German Research Foundation) under Germany's Excellence Strategy—EXC 2033—390677874—RESOLV. The simulations have been carried out at LRZ München (SuperMUC and SuperMUC-NG), HPC@ZEMOS, HPC-RESOLV, and BOVILAB@RUB.

*sho.imoto@theochem.rub.de

[1] K. D. Kreuer, S. J. Paddison, E. Spohr, and M. Schuster, Chem. Rev. **104**, 4637 (2004).
[2] Y. Zhang, J. Li, L. Ma, W. Cai, and H. Cheng, Energy Technol. **3**, 675 (2015).
[3] E. Quartarone, S. Angioni, and P. Mustarelli, Materials **10**, 687 (2017).
[4] D. Marx, A. Chandra, and M. E. Tuckerman, Chem. Rev. **110**, 2174 (2010).
[5] N. Agmon, H. J. Bakker, R. K. Campen, R. H. Henchman, P. Pohl, S. Roke, M. Thämer, and A. Hassanali, Chem. Rev. **116**, 7642 (2016).
[6] T. E. DeCoursey, Physiol. Rev. **93**, 599 (2013).
[7] M. Grote, M. Engelhard, and P. Hegemann, Bioenergetics **1837**, 533 (2014).
[8] A. Chandra, M. E. Tuckerman, and D. Marx, Phys. Rev. Lett. **99**, 145901 (2007).
[9] T. C. Berkelbach, H.-S. Lee, and M. E. Tuckerman, Phys. Rev. Lett. **103**, 238302 (2009).
[10] C. Dellago, M. M. Naor, and G. Hummer, Phys. Rev. Lett. **90**, 105902 (2003); **91**, 139902(E) (2003).
[11] D. J. Mann and M. D. Halls, Phys. Rev. Lett. **90**, 195503 (2003).
[12] C. Dellago and G. Hummer, Phys. Rev. Lett. **97**, 245901 (2006).
[13] M. Sharma, M. Yi, H. Dong, H. Qin, E. Peterson, D. D. Busath, H.-X. Zhou, and T. A. Cross, Science **330**, 509 (2010).
[14] B. Musset, M. E. Smith, S. Rajan, D. Morgan, V. V. Cherny, and T. E. DeCoursey, Nature (London) **480**, 273 (2011).
[15] S. Hu, M. Lozada-Hidalgo, F. Wang, A. Mishchenko, F. Schedin, R. Nair, E. Hill, D. Boukhvalov, M. Katsnelson, R. Dryfe *et al.*, Nature (London) **516**, 227 (2014).
[16] J. L. Achtyl, R. R. Unocic, L. Xu, Y. Cai, M. Raju, W. Zhang, R. L. Sacci, I. V. Vlassiouk, P. F. Fulvio, P. Ganesh *et al.*, Nat. Commun. **6**, 6539 (2015).
[17] D. Muñoz-Santiburcio, C. Wittekindt, and D. Marx, Nat. Commun. **4**, 2349 (2013).
[18] A. Bankura and A. Chandra, J. Chem. Phys. **142**, 044701 (2015).
[19] D. Muñoz-Santiburcio and D. Marx, Nat. Commun. **7**, 12625 (2016).
[20] D. Muñoz-Santiburcio and D. Marx, Phys. Rev. Lett. **119**, 056002 (2017).
[21] K. Gopinadhan, S. Hu, A. Esfandiar, M. Lozada-Hidalgo, F. Wang, Q. Yang, A. Tyurnina, A. Keerthi, B. Radha, and A. Geim, Science **363**, 145 (2019).
[22] A. K. Soper and M. A. Ricci, Phys. Rev. Lett. **84**, 2881 (2000).
[23] Th. Strässle, A. M. Saitta, Y. Le Godec, G. Hamel, S. Klotz, J. S. Loveday, and R. J. Nelmes, Phys. Rev. Lett. **96**, 067801 (2006).
[24] A. M. Saitta and F. Datchi, Phys. Rev. E **67**, 020201(R) (2003).
[25] S. Imoto, H. Forbert, and D. Marx, Phys. Chem. Chem. Phys. **17**, 24224 (2015).
[26] D. Marx and J. Hutter, *Ab Initio Molecular Dynamics: Basic Theory and Advanced Methods* (Cambridge University Press, Cambridge, 2009).
[27] See Supplemental Material at http://link.aps.org/supplemental/10.1103/PhysRevLett.125.086001 for computational details, validation of our approach, and additional analysis, which includes Refs. [28–51].
[28] J. Hutter, M. Iannuzzi, F. Schiffmann, and J. VandeVondele, Comput. Mol. Sci. **4**, 15 (2014).
[29] J. VandeVondele, M. Krack, F. Mohamed, M. Parrinello, T. Chassaing, and J. Hutter, Comput. Phys. Commun. **167**, 103 (2005).
[30] B. Hammer, L. B. Hansen, and J. K. Nørskov, Phys. Rev. B **59**, 7413 (1999).
[31] M. A. Marques, M. J. Oliveira, and T. Burnus, Comput. Phys. Commun. **183**, 2272 (2012).
[32] S. Grimme, J. Antony, S. Ehrlich, and H. Krieg, J. Chem. Phys. **132**, 154104 (2010).
[33] T. Morawietz, A. Singraber, C. Dellago, and J. Behler, Proc. Natl. Acad. Sci. U.S.A. **113**, 8368 (2016).
[34] P. Schienbein and D. Marx, J. Phys. Chem. B **122**, 3318 (2018).
[35] G. Lippert, J. Hutter, and M. Parrinello, Mol. Phys. **92**, 477 (1997).
[36] Y. Marcus, J. Chem. Phys. **137**, 154501 (2012).
[37] J. VandeVondele and J. Hutter, J. Chem. Phys. **127**, 114105 (2007).

[38] S. Goedecker, M. Teter, and J. Hutter, Phys. Rev. B **54**, 1703 (1996).
[39] C. Hartwigsen, S. Gœdecker, and J. Hutter, Phys. Rev. B **58**, 3641 (1998).
[40] W. Wagner and A. Pruß, J. Phys. Chem. Ref. Data **31**, 387 (2002).
[41] S. Woutersen and H. J. Bakker, Phys. Rev. Lett. **96**, 138305 (2006).
[42] S. T. Roberts, P. B. Petersen, K. Ramasesha, A. Tokmakoff, I. S. Ufimtsev, and T. J. Martinez, Proc. Natl. Acad. Sci. U.S.A. **106**, 15154 (2009).
[43] M. Thämer, L. De Marco, K. Ramasesha, A. Mandal, and A. Tokmakoff, Science **350**, 78 (2015).
[44] F. Dahms, R. Costard, E. Pines, B. Fingerhut, E. T. J. Nibbering, and T. Elsaesser, Angew. Chem. Int. Ed. **55**, 10600 (2016).
[45] F. Dahms, B. P. Fingerhut, E. T. Nibbering, E. Pines, and T. Elsaesser, Science **357**, 491 (2017).
[46] J. A. Fournier, W. B. Carpenter, N. H. C. Lewis, and A. Tokmakoff, Nat. Chem. **10**, 932 (2018).
[47] S. Imoto, P. Kibies, C. Rosin, R. Winter, S. M. Kast, and D. Marx, Angew. Chem. Int. Ed. **55**, 9534 (2016).
[48] M. Heyden, J. Sun, S. Funkner, G. Mathias, H. Forbert, M. Havenith, and D. Marx, Proc. Natl. Acad. Sci. U.S.A. **107**, 12068 (2010).
[49] D. Marx, M. E. Tuckerman, J. Hutter, and M. Parrinello, Nature (London) **397**, 601 (1999).
[50] D. Marx, Chem. Phys. Chem. **7**, 1848 (2006).
[51] M. E. Tuckerman, A. Chandra, and D. Marx, Acc. Chem. Res. **39**, 151 (2006).
[52] L. Skinner, M. Galib, J. Fulton, C. Mundy, J. Parise, V.-T. Pham, G. Schenter, and C. Benmore, J. Chem. Phys. **144**, 134504 (2016).
[53] M. Galib, M. Baer, L. Skinner, C. Mundy, T. Huthwelker, G. Schenter, C. Benmore, N. Govind, and J. L. Fulton, J. Chem. Phys. **146**, 084504 (2017).
[54] M. E. Tuckerman, D. Marx, and M. Parrinello, Nature (London) **417**, 925 (2002).
[55] S. Imoto and D. Marx, J. Chem. Phys. **150**, 084502 (2019).
[56] H. Vondracek, S. Imoto, L. Knake, G. Schwaab, D. Marx, and M. Havenith, J. Phys. Chem. B **123**, 7748 (2019).